# Controlled Source Audio-frequency Magnetotelluric (CSAMT) and Time Domain Electromagnetic (TDEM) Resistivity Measurements at Noboribetsu Geothermal Field, Kuttara Volcano, Hokkaido, Japan

Yoshihiko Goto* and Akira Johmori**

Controlled source audio-frequency magnetotelluric (CSAMT) and time domain electromagnetic (TDEM) resistivity measurements were performed in April 2008 at the Noboribetsu Geothermal Field, Kuttara Volcano, Hokkaido, Japan. Both sets of measurements were carried out using a high-precision electromagnetic system, Geo-SEM, controlled by GPS (Global Positioning System). The $2\times2$ km survey area covered the entire geothermal field and included 66 measurement sites. Interpretation of the CSAMT and TDEM data revealed the subsurface resistivity structure shallower than 1,400 m below sea level (b.s.l.). The most prominent feature of the resistivity structure is a region of low resistivity ($<10\,\Omega\cdot$m) beneath the geothermal field. The low resistivity varies in lateral extent and outline at different depths. At 200 m above sea level, it comprises two domains with long axes oriented NNW–SSE. From 0 to 200 m b.s.l., the two resistivity lows combine, forming a large semicircular low of $1,500\times1,500$ m in lateral extent. From 400 to 600 m b.s.l., the low resistivity has an irregular outline and includes linear low-resistivity zones trending NNW–SSE and ENE–WSW. From 800 to 1,400 m b.s.l., a linear NNW–SSE-trending region of low resistivity is apparent in an irregular overall pattern of resistivity. In a N–S vertical cross-section, the region of low resistivity extends vertically for more than 1,400 m. We attribute the low resistivity beneath the geothermal field to the presence of conductive clay minerals produced by hydrothermal alteration, which was in turn induced by high-temperature geothermal fluid ascending along fractures.

**Key words**: resistivity structure, controlled source audio-frequency magnetotelluric (CSAMT) survey, time domain electromagnetic (TDEM) survey, Noboribetsu Geothermal Field, Kuttara Volcano

## 1. Introduction

Resistivity surveying provides valuable information on underground geological structures at active volcanoes and within geothermal fields (*e.g*., Risk *et al*., 2003; Aizawa *et al*., 2008; Srigutomo *et al*., 2008). Such data are particularly useful for understanding hydrothermal systems, as the resistivity of volcanic rocks shows a marked change with the presence of alteration minerals and thermal waters. Resistivity data are therefore essential for scientific studies of volcanic activity and for geothermal exploration.

We performed controlled source audio-frequency magnetotelluric (CSAMT) and time domain electromagnetic (TDEM) resistivity measurements at Noboribetsu Geothermal Field, Kuttara Volcano, Hokkaido, Japan. The CSAMT method employed here used electric currents at frequencies from 1 to 8192 Hz. The TDEM method employed here was the long offset transient electromagnetic method (LOTEM; Strack, 1992). The Noboribetsu Geothermal Field is one of the major geothermal fields in Japan, and resistivity measurements are a promising tool for studying subsurface geologic structures within the geothermal field and for examining its hydrothermal systems. Sixty-six receiver stations were distributed in a $2\times2$ km area covering the whole geothermal field, and processing of the CSAMT and TDEM data revealed the subsurface resistivity structure shallower than 1,400 m below sea level (b.s.l.). This paper describes the results of the resistivity measurements and discusses the nature of subsurface geologic structures beneath the geothermal field.

## 2. Noboribetsu Geothermal Field

The Noboribetsu Geothermal Field lies in the western

*College of Environmental Technology, Graduate School of Engineering, Muroran Institute of Technology, Mizumoto-cho 27–1, Muroran, Hokkaido 050–8585, Japan.
**Neo Science Co., Ltd., Tarui 4–2–30, Sennan, Osaka 590–0521, Japan.

Corresponding author: Yoshihiko Goto
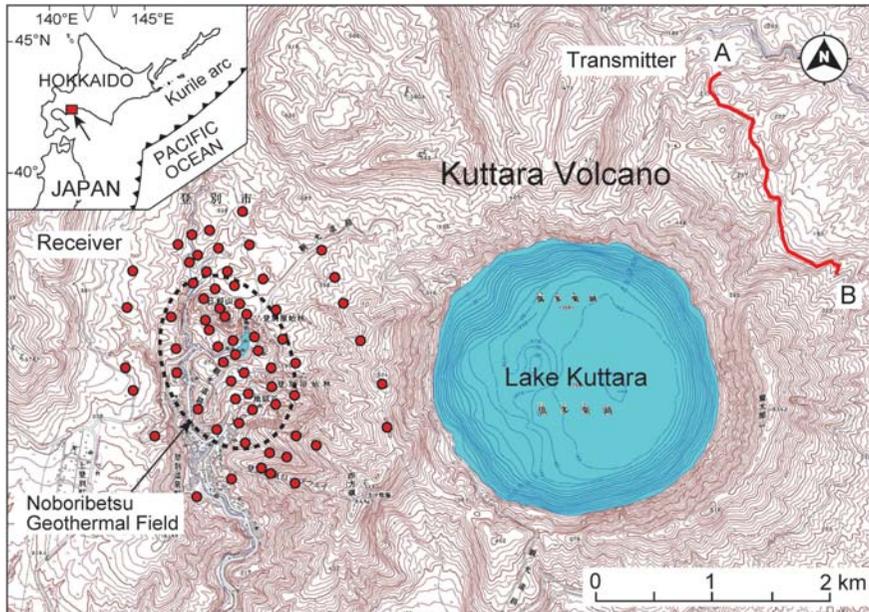e-mail: ygoto@mmm.muroran-it.ac.jp

Fig. 1. Location map of the Noboribetsu Geothermal Field at Kuttara Volcano, Hokkaido, Japan, showing the locations of the transmitter (line A–B) and receiver stations (red circles) for CSAMT and TDEM measurements. A and B are the ends of the dipole source. Topographic contour interval is 10 m.

part of Kuttara Volcano (Fig. 1), an andesitic to rhyolitic composite volcano (elevation, 549 m above sea level) with a small caldera at its summit (Lake Kuttara). The volcano evolved over the period 80–45 ka, involving early silicic explosive activity and subsequent stratovolcano building associated with caldera collapse at 40 ka (Katsui *et al.*, 1988; Yamagata, 1994; Moriizumi, 1998). The geothermal field, which is inferred to have formed after the collapse of the caldera (Katsui *et al.*, 1988), is approximately 1 km wide (NE–SW) and 1.5 km long (NW–SE), and occurs at an altitude of 200–370 m above sea level.

The Noboribetsu Geothermal Field is characterized by a dacitic cryptodome (Hiyoriyama Cryptodome), a volcanic lake (Oyunuma Lake), and a fumarolic valley (Jigokudani Valley) (Fig. 2A). The Hiyoriyama Cryptodome, in the northern part of the geothermal field, is elliptical in plan view (oriented NW–SE), is 350–550 m in diameter, and rises 130 m above the surrounding area. Its highest point is 377 m above sea level. The dome has a small explosion crater with active fumaroles at the summit. Oyunuma Lake (115×210 m in area), which is located in the central part of the geothermal field, is the largest lake in the field and is filled with hot acidic water. The Jigokudani Valley, in the southern part of the geothermal field, extends for 500 m in an ENE–WSW orientation and hosts active fumaroles. The geothermal manifestations of the geothermal field (active

fumaroles, hot springs, and hydrothermal alteration zones) are distributed in a zone extending NNE–SSW from the Hiyoriyama Cryptodome to the Jigokudani Valley.

The geology of the Noboribetsu Geothermal Field consists mainly of pyroclastic flow deposits derived from Kuttara Volcano (Moriizumi, 1998). The deposits are more than 200 m thick (NEDO, 1991) and are composed mainly of clasts of dacitic pumice (up to tens of centimeters across) in a cogenetic matrix. Faults in the geothermal field are oriented mainly NNW–SSE and ENE–WSW (Saito *et al.*, 1953). There are few published drilling data on the geothermal field (NEDO, 1991).

## 3. CSAMT and TDEM resistivity measurements
### 3–1  Electromagnetic system

CSAMT and TDEM resistivity measurements were performed using a high-resolution electromagnetic system (Geo-SEM; Neoscience Co., Ltd) consisting of a transmitter and receiver, both controlled by GPS (Figs. 3 and 4). The transmitter (Fig. 4A) consists of a transformer, rectifier, switching circuit, GPS clock, and a dipole source (grounded electrical source) that is 2 km long and that has 100 electrodes at each termination (Fig. 3). The transmitter is powered by separate generators for CSAMT and for TDEM (see Table 1 for specifications). The receiver (Fig. 4B) consists of an
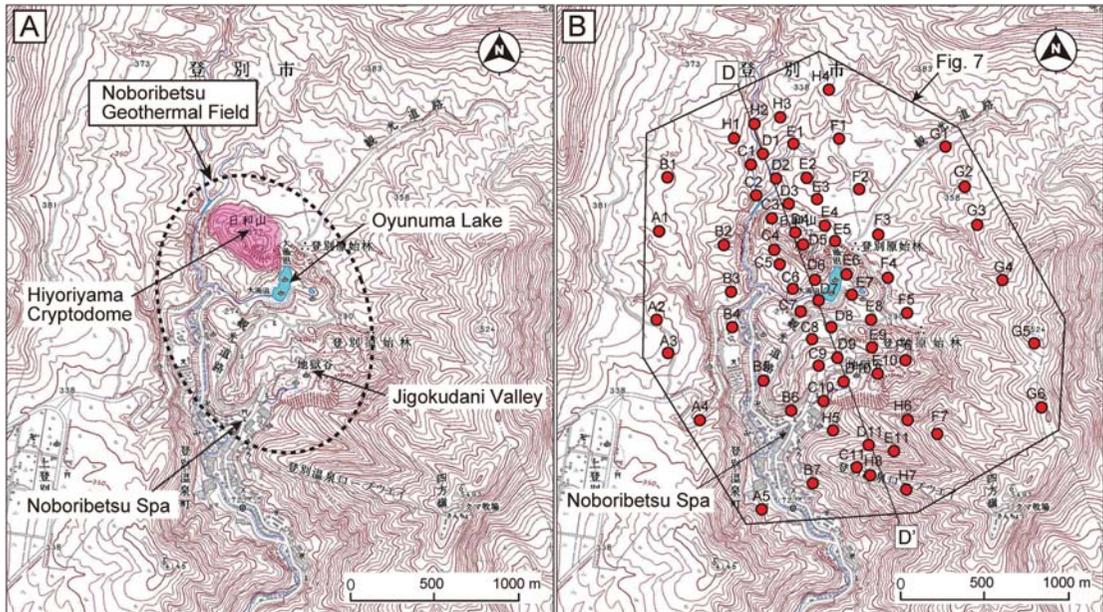
Fig. 2. (A) Topographic map showing the location of the Noboribetsu Geothermal Field. (B) Locations of receiver stations (red circles) for CSAMT and TDEM measurements over the Noboribetsu Geothermal Field. Also shown is the location of the vertical cross-section (D–D′) depicted in Fig. 8. Topographic contour interval is 10 m.

amplifier, filter, data logger, GPS clock, and sensor. The sensor consists of a pair of electrodes and coils, powered by a 12 V car battery. The transmitter and receiver are synchronized by a high-precision quartz clock system using GPS (accuracy, $1 \times 10^{-6}$ seconds). The specifications of the Geo-SEM system are listed in Table 1, and details of the system can be found in Johmori *et al.* (2010).

### 3–2 Measurements

The positions of the transmitter and receiver stations, used for both CSAMT and TDEM measurements, are shown in Figures 1 and 2. The transmitter was positioned 5 km northeast of the Noboribetsu Geothermal Field with its 2-km-long dipole source directed N30°W (Fig. 1). The receiver stations were located 4–6 km southwest of the transmitter (Fig. 1). The 66 receiver stations were distributed in a $2 \times 2$ km area covering the whole geothermal field (Fig. 2B).

The CSAMT/TDEM measurements were performed from 23 April to 25 May 2008. During the CSAMT measurements, the transmitter injected 1–8 A electric currents into the ground at frequencies of 1, 2, 4, 8, 16, 32, 64, 128, 256, 512, 1024, 2048, 4096, and 8192 Hz, and another series at frequencies of 20, 40, 80, 160, 320, 640, 1280, 2560, and 5120 Hz, in order to minimize the noise related to the commercial frequencies of 50 and 60 Hz and their higher harmonics. The receiver recorded the electric field parallel to the dipole source, and the

magnetic field perpendicular to the source. During the TDEM measurements, the transmitter injected 15 A electric currents into the ground in an 8-s cycle consisting of 2-s periods of 'on' and 'off', with alternating polarity. The receiver recorded the vertical magnetic response of the waveform at 40-$\mu$s intervals.

### 3–3 Data processing

The CSAMT data were processed using a band-pass filter, Fourier transform, and stacking, to remove noise. The stacking was performed >400,000 times at 8192 Hz or >300 times at 1 Hz. The apparent resistivity and phase were then calculated from the electric field and magnetic field. The TDEM data were stacked 500 times at most, rejecting the 50 Hz noise, and then smoothed using a moving average of 25 data points (40 $\mu$s $\times$ 25 data points = 1 ms). A transient response was then calculated by time integration of the smoothed data. The time integration was performed to obtain weightings for the low frequency data, which is suitable for analyses of deep resistivity structure. An example of TDEM data processing (for location D4) is shown in Figure 5.

### 3–4 Resistivity structure

The resistivity structure was calculated by one-dimensional (1D) joint inversion of the CSAMT and TDEM data at each measuring location. The apparent resistivity and phase angle of the CSAMT data, and the transient response of the TDEM data, were inverted to
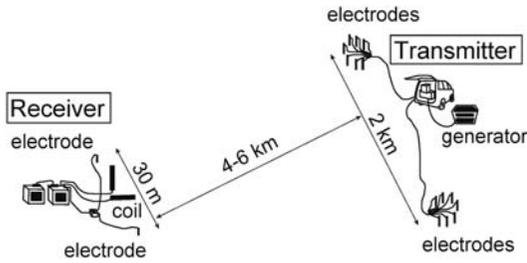
Fig. 3. Electromagnetic system (Geo-SEM) used for CSAMT and TDEM measurements. A pair of electrodes and a horizontal coil were used for CSAMT, whereas a vertical coil was used for TDEM.

Table 1. Specifications of the electromagnetic system (Geo-SEM) used for CSAMT and TDEM measurements.

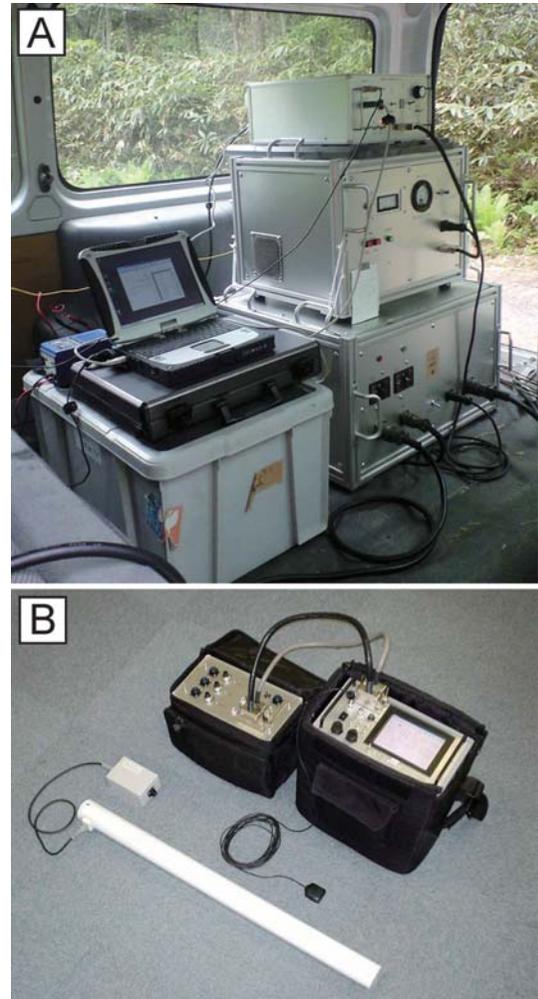| CSAMT | |
|---|---|
| Transmitter | |
| Output power | 5 kW (maximum) |
| Output voltage | 1000 V (maximum) |
| Output current | 10 A (maximum) |
| Frequency | 1, 2, 4, 8, 16, 32, 64, 128, 256, 512, 1024, 2048, 4096, 8192 Hz |
| | 20, 40, 80, 160, 320, 640, 1280, 2560, 5120 Hz |
| Generator | 6 kW (maximum), 200V AC, 60 Hz, 3 phase |
| Receiver | |
| Frequency | 1, 2, 4, 8, 16, 32, 64, 128, 256, 512, 1024, 2048, 4096, 8192 Hz |
| | 20, 40, 80, 160, 320, 640, 1280, 2560, 5120 Hz |
| Channel | 3 or 5 channels |
| Amplification degree | 0-90 dB (10 dB pitch) |
| Wave analysis | stacking, Fourier transform |
| TDEM | |
| Transmitter | |
| Output power | 25 kW (maximum) |
| Output voltage | 800 V (maximum) |
| Output current | 30 A (maximum) |
| Transmission time | 16, 8, 4, 2, 1, 0.8, 0.4, 0.2, 0.1 sec |
| Generator | 25 kW (maximum), 440V AC, 60 Hz, 3 phase |
| Receiver | |
| Sampling interval | 40 μsec |
| Channel | 3 or 5 channels |
| Amplification degree | 0-90 dB (10 dB pitch) |
| Wave analysis | stacking, digital filter |



Fig. 4. Photographs of the transmitter (A) and receiver (B) of the electromagnetic system (Geo-SEM) used in the CSAMT and TDEM measurements. The white coil for CSAMT measurements (as shown in B) is 72 cm long.

yield the resistivity structure, assuming a horizontal layered structure. Analytical theory for the layered structure was based on Ward and Hohmann (1987). The inversion was carried out by comparing the field data with the calculated results, using the nonlinear least-squares method (Fig. 6). The depth of penetration was determined by the sensitivity of the deepest layer to resistivity. We tested the sensitivity of the deepest layer to resistivity by doubling or halving the resistivity of the deepest layer and then checking the change in the root mean square (RMS) values obtained from the field data and from the calculated result. If the original RMS value showed no change, the deepest layer was interpreted to be insensitive to resistivity and the second-deepest layer was then examined.

The resistivity structure, obtained by the 1D joint inversion analysis, contained errors due to static shift and topographic effects. To reduce these errors, 2D analysis (cf., Sasaki, 1986) was performed employing the CSAMT data, using the finite element method and setting the result of the 1D analysis as the initial model. 2D resistivity structures were calculated along seven sections oriented NNW–SSE (A1–A5, B1–B7, C1–C11, D1–D11, E1–E11, F1–F7, and G1–G6 in Fig. 2). Finally, the 3D resistivity structure was produced from the seven 2D sections.

## 4. Results
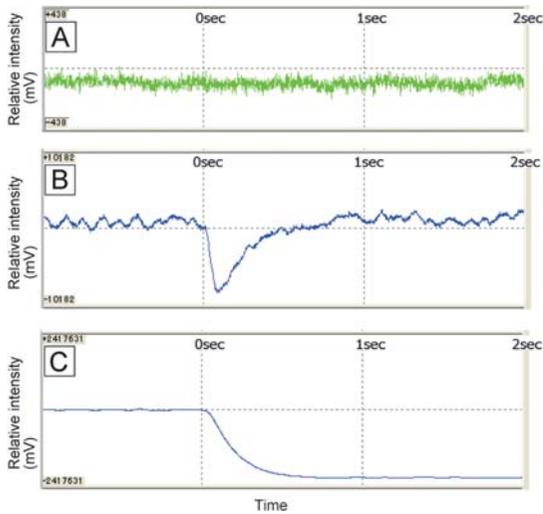Processing of the CSAMT and TDEM data revealed

Fig. 5. Example of TDEM-data processing (for location D4). (A) Raw TDEM data including noise. (B) TDEM data after stacking 402 times and smoothing. (C) Transient response produced by time integration.
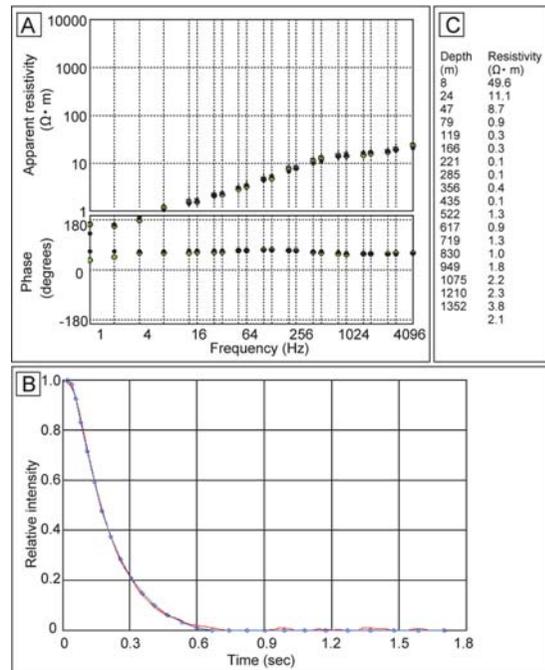


Fig. 6. Example of one-dimensional joint inversion at location D4. (A) Comparison of CSAMT field data (green circles) and calculated results (black circles). (B) Comparison of TDEM transient field data (red line) and calculated results (blue circles). (C) Calculated resistivity structure.

a subsurface resistivity structure shallower than 1,400 m b.s.l. (Figs. 7 and 8). Figure 7 shows horizontal sections of the resistivity structure at vertical intervals of 200 m. The most prominent feature of the resistivity structure is the presence of a region of low resistivity ($<10\,\Omega\cdot$m) beneath the geothermal field. In plan view, this region varies in lateral extent and outline at different depths. At the ground surface (Fig. 7A), two domains of low resistivity are recognized: a northern low at Oyunuma Lake (receiver stations D6 and D7) and a southern low at Jigokudani Valley (D10). These lows occur at similar locations to geothermal features such as hot springs, fumaroles, and hydrothermal alteration zones. At 200 m above sea level (Fig. 7B), the two lows combine to define a linear low-resistivity zone that extends for 1,500 m in a NNW–SSE orientation, with a width of 500 m. At sea level (Fig. 7C), the two lows are completely united, showing a semicircular or quadrangular shape that is 1,000 m across, centered at Oyunuma Lake (receiver station D7). At 200 m below sea level (Fig. 7D), the region of low resistivity is enlarged to an area of $1,500\times1,500$ m. From 400 to 600 m below sea level (Fig. 7E, F), the low shows a more irregular outline and appears to be an assemblage of linear low-resistivity zones trending NNW–SSE and ENE–WSW. From 800 to 1,400 m below sea level (Fig. 7G–J), a linear low-resistivity zone trending NNW–SSE (receiver stations D1–D9) is observed among an irregular overall pattern of resistivity.

Figure 8 shows a vertical cross-section of the resistivity structure along the line D–D′ (Fig. 2B). In the section, a region of low resistivity occurs beneath the geothermal field, centered at Oyunuma Lake and extending to 1,400 m depth below sea level.

## 5. Discussion

The resistivity of rocks and sediments is generally lowered by the presence of conductive minerals (*e.g.*, smectite-series clays), thermal water in pores and fractures, and high ground temperatures (*e.g.*, Risk *et al.*, 2003). In the Noboribetsu Geothermal Field, the region of low resistivity is located beneath geothermal features such as fumaroles, hot springs, and hydrothermal alteration zones, consistent with the presence of clay minerals produced by hydrothermal alteration related to upwelling high-temperature fluids and/or the presence of high-temperature, thermal water in porous or fractured rocks. In explaining the low resistivity, we favor a combination of the presence of clay minerals, thermal water, and high ground temperatures.

The low resistivity at 400–600 m below sea level (Fig. 7E and F) is irregular in outline and appears to be an
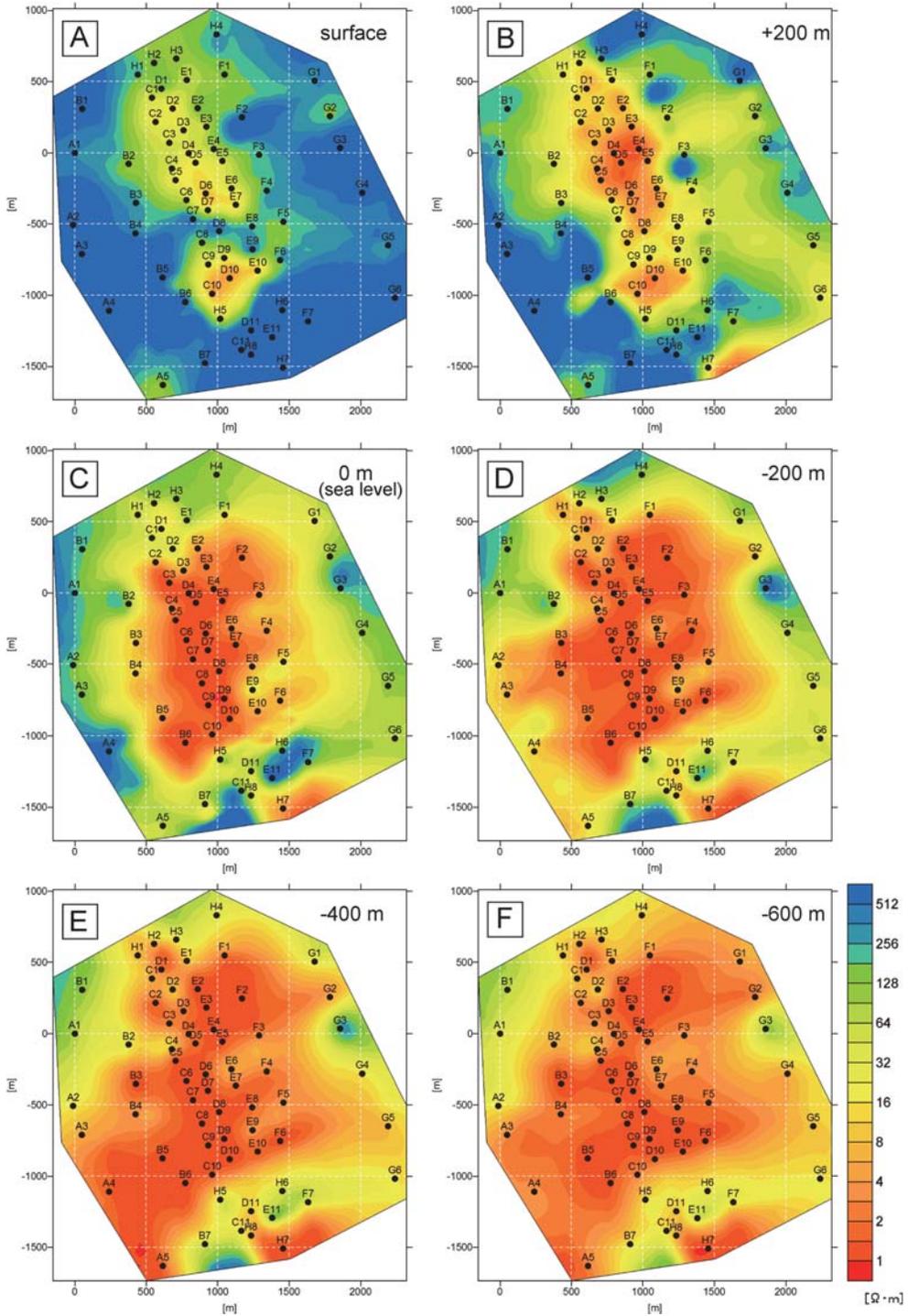
Fig. 7.   Horizontal resistivity pseudosections of the Noboribetsu Geothermal Field at a vertical interval of 200 m. The locations and numbers of receiver stations are shown in Fig. 2B.
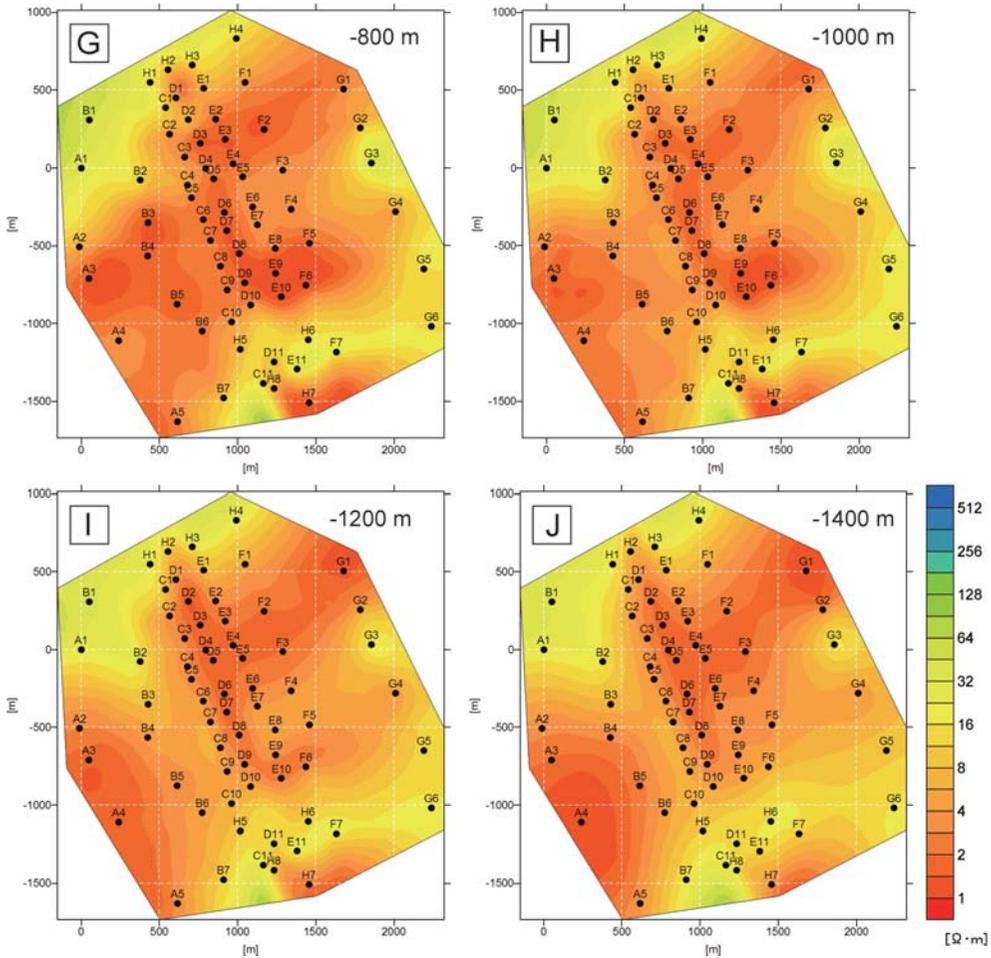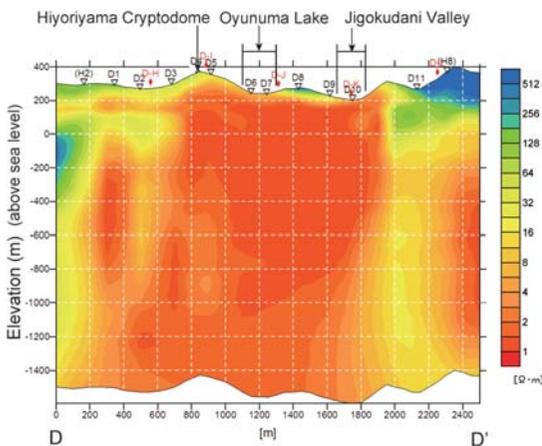
Fig. 7.   (continued)



Fig. 8.  Vertical resistivity pseudosection of the Noboribetsu Geothermal Field along the line D–D′ (see Fig. 2B).

assemblage of linear lows trending NNW–SSE and ENE–WSW, implying the presence of clay minerals and/or high-temperature geothermal fluid along fractures developed in these orientations.   These fractures would enable the upwelling of high-temperature fluid, causing hydrothermal alteration.   Faults in the Noboribetsu Geothermal Field are developed mainly in NNW–SSE and ENE–WSW orientations (Saito *et al*., 1953), indicating the linear lows are related to the presence of clay minerals and/or high-temperature geothermal fluid along faults at depth.

The linear NNW–SSE-trending low at 800–1,400 m below sea level (D1–D10 in Fig. 7G–J) is inferred to be related to deep fractures developed in this orientation. The low at this depth is similar in location to the low resistivity at the ground surface (D1–D10 in Fig. 7A, where geothermal features are located), suggesting that the surface features have developed above the deep fractures.   The fractures at 800–1,400 m below sea

level are therefore inferred to be important pathways for upwelling high-temperature fluids.

## References

Aizawa, K., Ogawa, Y., Hashimoto, T., Koyama, T., Kanda, W., Yamaya, Y., Mishima, M. and Kagitama, T. (2008) Shallow resisitivity structure of Asama volcano and its implications for magma ascent process in the 2004 eruption. *J. Volcanol. Geotherm. Res.* **173**, 165–177.

Johmori, A., Mitsuhata, Y., Nishimura, S., Johmori, N., Kondou, T. and Takahashi, T. (2010) Development of a deep electromagnetic exploration instrument with high frequency spectrum resolution using GPS synchronization. *Jour. Japan Soc. Engin. Geol.,* **51**, 62–72. (in Japanese with English abstract)

Katsui, Y., Yokoyama, I., Okada, H., Abiko, T. and Muto, H. (1988) **Kuttara (Hiyoriyama), its volcanic geology, history of eruption, present state of activity and prevention of disasters**. Committee for Prevention and Disasters of Hokkaido, Sapporo, 99p. (in Japanese)

Moriizumi, M. (1998) The growth history of the Kuttara volcanic group. *Bull. Volcanol. Soc. Japan,* **43**, 95–111. (in Japanese with English abstract)

NEDO (New Energy and Industrial Technology Development Organization) (1991) **Noboribetsu, Report of promotional exploration for geothermal research**, No. 22. NEDO, Tokyo, 845p. (in Japanese)

Risk, G.F., Caldwell, T.G. and Bibby, H.M. (2003) Tensor time domain electromagnetic resistivity measurements at Ngatamariki geothermal field, New Zealand. *J. Volcanol. Geotherm. Res.* **127**, 33–54.

Saito, M., Osanai, H. and Sako, S. (1953) **Explanatory text of the Geological map of Japan, scale 1 : 50000, Noboribetsuonsen**. Geological Survey of Hokkaido, 84p. (in Japanese with English abstract)

Sasaki, Y. (1986) Resolving power of MT method for two-dimensional structures. *Geophysical Exploration,* **39**, 1–9.

Srigutomo, W., Kagiyama, T., Kanda, W., Munekane, H., Hashimoto, T., Tanaka, Y., Utada, H. and Utsugi, M. (2008) Resistivity structure of Unzen volcano derived from time domain electromagnetic (TDEM) survey. *J. Volcanol. Geotherm. Res.* **175**, 231–240.

Strack, K.M. (1992) **Exploration with deep transient electromagnetics. Elsevier, Amsterdam. 373p.**

Ward, S.H. and Hohmann, G.W. (1987) Electromagnetic theory for geophysical applications. In : *Electromagnetic methods in applied geophysics* (Nabighian, M. ed), 131–311, Society of Exploration Geophysicists (SEG), Oklahoma.

Yamagata, K. (1994) Tephrochronological study on the Shikotsu and Kuttara Volcanoes in southwestern Hokkaido, Japan. *J. Geogr.,* **103**, 268–285. (in Japanese with English abstract)

(Editional handling Takeshi Hashimoto)

# 北海道南西部クッタラ火山，登別地熱地域の CSAMT・TDEM 法による比抵抗構造探査

後藤芳彦・城森　明

　北海道南西部クッタラ火山登別地熱地域において，CSAMT 法および TDEM 法の電磁探査を行い，地下 1400 m までの比抵抗構造を解明した．探査は登別地熱地域を含む 2×2 km の範囲で行い，受信点は 66 箇所に配置した．解析は CSAMT・TDEM データのジョイント一次元逆解析および CSAMT データを用いた二次元逆解析で行った．その結果，登別地熱地域の直下に，低比抵抗領域 (＜10Ω・m) が存在することが明らかになった．低比抵抗領域は，直径 1500×1500 m で，鉛直方向に 1400 m 以上伸長する．この低比抵抗領域は，高温の地熱流体が地下割れ目を上昇して形成された熱水変質帯，地下割れ目に存在する高温の地熱流体，および高い地下温度を示すと考えられる．